



JAEA-Review
2012-036

Reports on JAEA's Reimei Research Program
April 1, 2011 – March 31, 2012

(Ed.) Yuichiro NAGAME

Advanced Science Research Center

JAEA-Review

October 2012

Japan Atomic Energy Agency

日本原子力研究開発機構

本レポートは独立行政法人日本原子力研究開発機構が不定期に発行する成果報告書です。
本レポートの入手並びに著作権利用に関するお問い合わせは、下記あてにお問い合わせ下さい。
なお、本レポートの全文は日本原子力研究開発機構ホームページ (<http://www.jaea.go.jp>)
より発信されています。

独立行政法人日本原子力研究開発機構 研究技術情報部 研究技術情報課
〒319-1195 茨城県那珂郡東海村白方白根 2 番地 4
電話 029-282-6387, Fax 029-282-5920, E-mail:ird-support@jaea.go.jp

This report is issued irregularly by Japan Atomic Energy Agency
Inquiries about availability and/or copyright of this report should be addressed to
Intellectual Resources Section, Intellectual Resources Department,
Japan Atomic Energy Agency
2-4 Shirakata Shirane, Tokai-mura, Naka-gun, Ibaraki-ken 319-1195 Japan
Tel +81-29-282-6387, Fax +81-29-282-5920, E-mail:ird-support@jaea.go.jp

© Japan Atomic Energy Agency, 2012

Reports on JAEA's Reimei Research Program
April 1, 2011 – March 31, 2012

(Ed.) Yuichiro NAGAME

Advanced Science Research Center
Japan Atomic Energy Agency
Tokai-mura, Naka-gun, Ibaraki-ken

(Received August 27, 2012)

The Reimei (Dawn) Research Program is conducted based on public application to encourage original and/or unique ideas in the field of new frontier research on atomic energy sciences. Candidates for the offering have been extended beyond the country since the fiscal year of 2010. The five research subjects including three ongoing ones were accepted in the fiscal year 2011 that were carried out in collaboration with Advanced Science Research Center. The three successive projects, in particular, have achieved substantial progress through the effective international collaboration. The summaries of these research subjects are compiled in this report. We hope that new frontier research projects will be developed through the present Reimei Research Program.

Keywords: Reimei Research Program, Atomic Energy Science

平成 23 年度黎明研究成果報告集

日本原子力研究開発機構 先端基礎研究センター
(編) 永目 諭一郎

(2012 年 8 月 27 日受理)

原子力科学の分野で革新的な原理や現象の発見をめざす先端基礎研究を対象として、研究テーマを原子力機構外から公募する黎明研究制度が平成 18 年度から新たに発足した。研究期間を最長 2 年間とし、年度ごとに評価を実施して課題を採択することとした。平成 22 年度からは応募対象を国外にも広げ、国際共同研究へと発展させている。平成 23 年度は、応募総数 27 件の中から継続課題 3 件を含む 5 件を選定し、先端基礎研究センターとの共同研究として実施した。特に継続の 3 課題は大きな進展を遂げており、国際共同研究による研究交流が効果的に機能している。

本報告書は、黎明研究から多くの基礎・基盤研究が進展する一助とするため、黎明研究の実施者より提出された成果報告書をまとめ、公表するものである。

Contents

| | | |
|---|---|----|
| 1 | New Approach to the Exotic Phases of Actinide Compounds under Unconventional Experimental Conditions · · · · · | 1 |
| | A. Hiess and G. H. Lander | |
| 2 | New Fission Mechanism Peculiar to Proton-rich Nuclei · · · · · | 9 |
| | A. Andreyev, K. Nishio, X. Derkx, J. Lane, V. Liberati, K. Sandhu, S. Chiba, S. Mitsuoka, I. Nishinaka, H. Makii, Y. Wakabayashi, Y. Aritomo, S. Ota, T. Nagayama, L. Ghys, T. Ohtsuki, IS466 and ISOLDE Collaboration | |
| 3 | Exploration of New Biological Specific Function by Heavy Elements Stimulus · · · · · | 14 |
| | L. Macaskie, J. Renshaw, T. Ohnuki, N. Nishiguchi, S. Utsunomiya, Y. Suzuki and O. Shirai | |
| 4 | Synthesis, Magnetic and Transport Studies of Li(Zn,Mn)As and Other Doped I-II-V Magnets · · · · | 19 |
| | Z. Deng, C. Q. Jin, Q. Q. Liu, X. C. Wang, J. L. Zhu, S. M. Feng, L. C. Chen, R. C. Yu, C. Arguello, T. Goko, Fanlong Ning, Jinsong Zhang, Yayu Wang, A. A. Aczel, T. Munsie, T. J. Williams, G. M. Luke, T. Imai, T. Kakeshita, S. Uchida, W. Higemoto, T. U. Ito, Bo Gu, S. Maekawa, G. D. Morris, W.Q. Yu and Y. J. Uemura | |
| 5 | Theory of Spintronics and Materials: Mechanisms and Applications of the Spin Hall Effect, Multiferroics and Muon Spintronics · · · · · | 24 |
| | T. Ziman and M. Mori | |

目 次

| | | |
|---|--|----|
| 1 | 極限条件下実験によるアクチノイド化合物のエキゾチック物性研究への新しい アプローチ 1 A. Hiess and G. H. Lander | 1 |
| 2 | 陽子過剰核の新しい核分裂過程 9 A. Andreyev, K. Nishio, X. Derkx, J. Lane, V. Liberati, K. Sandhu, S. Chiba, S. Mitsuoka, I. Nishinaka, H. Makii, Y. Wakabayashi, Y. Aritomo, S. Ota, T. Nagayama, L. Ghys, T. Ohtsuki, IS466 and ISOLDE Collaboration | 9 |
| 3 | 重元素刺激による微生物の特異な機能の探索 14 L. Macaskie, J. Renshaw, T. Ohnuki, N. Nishiguchi, S. Utsunomiya, Y. Suzuki and O. Shirai | 14 |
| 4 | Li(Zn,Mn)As 及び他のドーパされた I-II-V 族磁性体の合成、磁性および輸送特性の研究 . . . 19 Z. Deng, C. Q. Jin, Q. Q. Liu, X. C. Wang, J. L. Zhu, S. M. Feng, L. C. Chen, R. C. Yu, C. Arguello, T. Goko, Fanlong Ning, Jinsong Zhang, Yayu Wang, A. A. Aczel, T. Munsie, T. J. Williams, G. M. Luke, T. Imai, T. Kakeshita, S. Uchida, W. Higemoto, T. U. Ito, Bo Gu, S. Maekawa, G. D. Morris, W. Q. Yu and Y. J. Uemura | 19 |
| 5 | スピントロニクスおよびその材料に関する理論：スピンホール効果、マルチフェロイクス およびミュオンスピントロニクスのメカニズムと応用 24 T. Ziman and M. Mori | 24 |

1. New Approach to the Exotic Phases of Actinide Compounds under Unconventional Experimental Conditions

A. Hiess^{1,*} and G. H. Lander^{1,2}

¹ Institut Laue–Langevin, Grenoble, France

² European Commission, Institute for Transuranium Elements, JRC, Karlsruhe, Germany

Abstract

We describe some collaborative experiments using large facilities that have been performed during the second year of the REIMEI project with the title above. Also discussed are the conclusions of the 2nd Workshop on this program, held at the Institut Laue Langevin, Grenoble, France, 1–3 Feb. 2012.

1. Research Objectives

We propose development of measurements for actinides compounds under unconventional conditions *i.e.* radioactive (uranium, transuranium, ²³⁵U enriched) samples, high magnetic field, and high pressures on international collaborations of several institutes which have their own special techniques, in order to discover and clarify the exotic electronic properties in 5f-electron

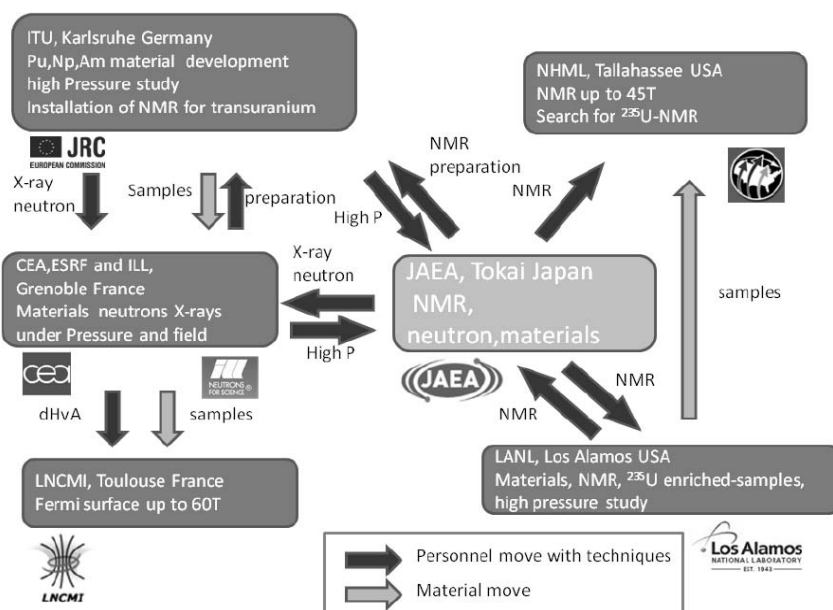


Fig. 1 Organization of international collaboration

systems, which appear only under extreme conditions due to large energy scales (Fermi energy, Kondo temperature), compared with 4f-systems. A special emphasis will be put to combine in-situ bulk measurements with scattering methods to gain microscopic insight into the various phases in such systems. Because of the difficulty for international transport of actinides samples, researchers and experimental methods will be encouraged to travel and collaborate to develop and perform the investigations. The collaborative aspect of the project may be illustrated in Fig. 1.

2. Research Contents

We describe below some of the collaborations that have been extended in the second year of operating the REIMEI project.

- (1) High magnetic field NMR using ^{29}Si -enriched URu_2Si_2 in NHMFL, USA. Collaboration among JAEA, LANL and NHMFL underway at NHMFL.
- (2) Observation of the ^{239}Pu NMR signal in PuO_2 . Collaboration between LANL and JAEA.
- (3) Work has been carried out on a new Pu-superconductor, PuCoIn_5 as part of a collaboration between LANL and ITU.
- (4) Chirality of the spin resonance excitation in an unconventional superconductor. Collaboration between ILL and JAEA.
- (5) NMR in 115 and 127 materials. Collaboration between LANL and JAEA.
- (6) Dynamics of UO_2 at low temperature. Collaboration between ITU and ILL.
- (7) Mössbauer-effect measurements on NpFeGa_5 . Collaboration between ITU and CEA.
- (8) Understanding the complex phase diagram of uranium: the role of electron-phonon coupling. Collaboration between CEA, ITU, and LANL.
- (9) Second International REIMEI Workshop at the Institut Laue Langevin, Grenoble, France, 1–3 Feb. 2012
- (10) New in-sights combining in-situ AC (alternating current) susceptibility measurements with neutron spectroscopy.

3. Research results

- (1) *High magnetic field NMR using ^{29}Si -enriched URu_2Si_2 in NHMFL.*

Several single crystals of URu_2Si_2 enriched to 99.8 at. % by the ^{29}Si isotope were prepared, which can reduce the measurement time very efficiently. These samples were shipped from LANL to NHMFL. The crystals were grown by the Czochralski-pulling method, and well annealed with a solid-state electro-transport furnace under ultra high vacuum condition. In the first NMR measurement by the JAEA and NHMFL NMR groups, we have characterized the sample quality, which is in fact consistent with the previously reported line width in a non-enriched sample. For the next measurement in the higher field, we will concentrate to measure the temperature dependence of a NMR spectrum under the several higher fields up to 29 T, in order to identify the phase transition around 22 T, which would be accompanied with a change of Fermi-surface. In recent measurements up to 40T, we have confirmed the anomaly at 22 T in the Knight shift, and found a strong increase of Knight from 29 T to 35 T where a 1st order phase transition takes place. At 35 T, we have

lost the signal due to a sudden change of the Knight shift, which indicates a large change of the density of state at the transition. In addition to the high field NMR study, we have developed high pressure NMR cell in order to perform NMR under multi-extreme (high H+ high P) conditions.

(2) *Discovery of ^{239}Pu NMR signal in PuO_2 .*

In a collaboration between JAEA and LANL the signal from the $s = 1/2$ nucleus of ^{239}Pu has been found for the first time in a sample of PuO_2 cooled to 4.2 K, as shown in Fig. 2.

It is important to observe a ^{239}Pu -NMR signal since we can investigate the behavior of the 5f-electrons directly by this method. NMR signals of actinide nuclei have been searched for many years, but it has been successful only for ^{235}U -NMR previously. Due to the synthesise of a very pure $^{239}\text{PuO}_2$ sample in LANL, the first ^{239}Pu -NMR signal has been observed. So far, the gyro-magnetic ratio for the ^{239}Pu -nucleus has not been determined precisely. This measurement has determined it as 2.8 MHz/ μ_B . This observation opens a new aspect for chemistry and physics in Pu complexes and compounds. This work has been published in ref. [1].

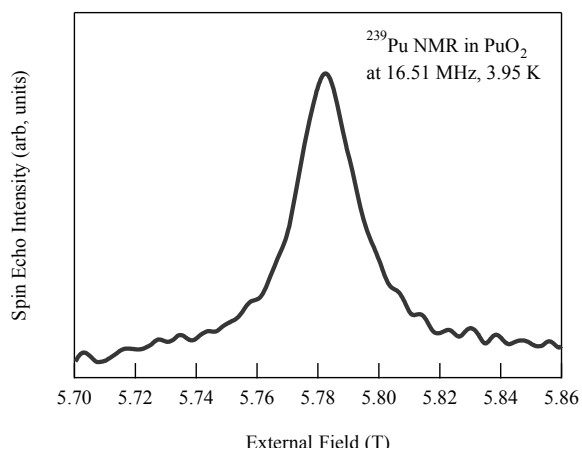


Fig. 2 ^{239}Pu NMR of PuO_2 (Spin-echo) field swept spectra taken at 16.51 MHz and 3.95K .

(3) *Discovery and characterization of a new Pu-based superconductor, PuCoIn_5 .*

In a collaboration between LANL and ITU, single crystals of this material have been characterized. The 5f electrons in PuCoIn_5 ($T_c = 2.5$ K) appear more localized than those in PuCoGa_5 ($T_c = 18.5$ K), and there is no antiferromagnetic(AF) ordering observed. The physical properties indicate that the spin-fluctuation energy scale of PuCoIn_5 is 3–4 times smaller than that of PuCoGa_5 due to a 28% larger unit cell volume, suggesting that the Pu 5f electrons are in a more localized state in PuCoIn_5 than in PuCoGa_5 . Electrical resistivity measurements under pressure on PuCoIn_5 will be useful for determining whether there are two superconducting domes or whether PuCoGa_5 and PuCoIn_5 reside on the same broad superconducting dome located near an AF quantum critical point and have a common pairing mechanism. This work has been published in ref. [2].

(4) *Chirality of the spin resonance excitation in an unconventional superconductor.*

As in the case of high temperature superconductors, the spin dynamics changes on entering the superconducting state in cerium- and uranium-based intermetallic superconductors such as CeCoIn_5 , CeCu_2Si_2 , UPd_2Al_3 and UPd_2Al_3 . Inelastic neutrons scattering experiments reveal a magnetic response in the normal state at specific

momentum space positions. On entering the superconducting state a gap opens at low energies and an increased magnetic intensity is present above the gap, forming in most cases a sharp ‘spin resonance’. Using the IN14 spectrometer at ILL we investigated the polarization dependence of the inelastic peak present at $(1/2, 1/2, 1/2)$ in CeCoIn₅ under an applied magnetic field. We show that the spin resonance of the heavy fermion superconductor CeCoIn₅ is a degenerate mode and that Zeeman splitting occurs, a feature specific of Pauli limited superconductors. Beside the Zeeman split contribution which exhibits a chiral character, a longitudinal-like mode is evidenced and both contributions have similar spectroscopic g-factors. We now obtained beam time on the IN14 at ILL to perform a similar investigation using the antiferromagnetically ordered superconductor UPd₂Al₃ ($T_N = 14$ K, $T_c = 2$ K). The signal at the AF position $(0, 0, 1/2)$ has been extensively studied with unpolarized and polarized neutrons. The latter confirms that the intensity is exclusively of magnetic origin. We expect our experiment to answer two questions: Is the ‘spin resonance’ in UPd₂Al₃ a degenerate mode? Is the underlying anisotropy similar to CeCoIn₅?

This work has been submitted for publication [3].

(5) *NMR in 115 and 127 materials*

In a collaborative study between JAEA and LANL a number of so-called 115 and 127 compounds have been studied by NMR and bulk techniques. In the heavy-fermion superconductor CeCoIn₅, quantum criticality is observed around the upper critical field H_{c2} at $T = 0$, which is reported for macroscopic properties such as specific heat. However, the origin of this quantum criticality has never been identified. The temperature dependence of the spin-lattice relaxation time T_1 has been measured for several different fields at low temperatures [4]. At an applied magnetic field of H_{c2} at $T = 0$, $1/T_1 T$, which is proportional to the magnetic dynamical susceptibility, increases rapidly with decreasing T i.e. approaching the H_{c2} point. On the other hand, such prominent increase of $1/T_1 T$ has not been observed at different magnetic fields. This fact confirms that the quantum criticality at H_{c2} in CeCoIn₅ is due to magnetic instability.

The crystal structure of heavy fermion CePt₂In₇ is similar to the 115 structure. In this compound AF ordering is suppressed under pressure and superconductivity appears. The antiferromagnetically ordered structure has been determined as an incommensurate one by means of NMR at the zero field [5]. In addition, an incommensurate to commensurate modification of the ordering structure is observed with increasing pressure. This behavior is quite similar to that of CeRhIn₅, which also shows superconductivity under pressure. Now, a study of the superconducting state under pressure is in progress.

(6) *Dynamics of UO₂ at low temperature.*

This work has been performed on collaboration among ITU, ILL, and the University of Parma, Italy. In this work, a complete understanding of the dynamics of UO₂ is given based on quadrupolar related excitations after an effort that has lasted many years [6]. The results are in very good agreement with the predictions of mean-field random phase

approximation calculations, emphasizing the importance of multipolar super-exchange interactions. By comparing neutron scattering intensities in different polarization channels and at equivalent points in different Brillouin zones, we show the mixed magneto-vibrational quadrupolar character of the observed excitations. The high-energy resolution afforded by the cold triple-axis spectrometer allowed us to study in detail the magnon-phonon interaction giving rise to avoided crossings along the $[00\xi]$ reciprocal space direction.

(7) *Mössbauer effect measurements on NpFeGa₅*

This work has been performed on collaboration between CEA and ITU. NpFeGa₅ single crystals prepared by the Ga-flux method have been investigated by magnetization, specific heat and ²³⁷Np Mössbauer spectroscopy measurements. An AF transition has been observed at $T_N \sim 114$ K. The second AF transition, which takes place at $T^* \sim 74$ K has only been detected in the magnetization data. A saturated ordered Np moment of 1.00(5) μ_B and the occurrence of an Np³⁺ charge state were inferred from the Mössbauer data. The angle between the Np ordered moment and the basal plane was shown to be $\sim 17^\circ$, in good agreement with the value observed by neutron diffraction in the low temperature AF phase. The absence of change of the quadrupole interaction parameters at T^* did not allow us to gain information on the Np moment reorientation at T^* . The trend of the isomer shift along the NpTGa₅ series and the discrepancy between the Np moments determined by neutron diffraction and Mössbauer spectroscopy indicates a partial spatial delocalisation of the 5f electrons in NpFeGa₅. This work has been published [7].

(8) *Understanding the complex phase diagram of uranium: the role of electron-phonon coupling.*

This work represents a collaboration among CEA, ITU, LANL, and ESRF. It was discussed in the last report, and the paper has now been published [8].

(9) *Second International REIMEI Workshop at the Institut Laue Langevin, Grenoble, France, 1–3 Feb. 2012.*

Some 40 scientists attended this Workshop, and discussed current problems associated with actinide materials, as well as the large number of collaborations that exist between different members of the REIMEI Group. The largest contingent was from Japan, some 14 scientists, most from the JAEA Tokai site. 14 scientists from the Grenoble region, most at the CEA, also attended. 4 came from ITU, Germany, and 3 from the USA. 5 others from different parts of Europe also attended. All received at least some support from the REIMEI program.

The meeting started with an account of current research projects at the four major centers involved in this work; CEA (J–P. Brison), ITU (R. Caciuffo), JAEA (S. Kambe), and LANL (J. D. Thompson) bringing us up to date with both capabilities and collaborations. Over the next 3 days we had a total of 24 talks by participants, and a lively poster session.

Among the highlights of the meeting was the discussion of the new Pu-based superconductor PuCoIn₅ ($T_c = 2.5$ K), discovered at LANL. Initially, this material was thought to have AF ordering, but a collaborative program between LANL and ITU has established that the AF ordering is from an impurity phase. Experiments have shown that the 5f electrons in PuCoIn₅ are considerably more localized than in the PuCoGa₅ ($T_c = 18.5$ K) material. Another major highlight from H. Yasuoka (JAEA) was the discovery at LANL of the ²³⁹Pu NMR signal in PuO₂ at 4.2 K – a signal that has been sought for 50 years. This was a joint LANL – JAEA success, and is now published in *Science*. There was a two-session discussion of the famous “hidden-order” in URu₂Si₂. But despite considerable efforts, the detailed physics behind this transition remains “hidden”!

J. D. Thompson (LANL) discussed possible “heterogeneity” in both 4f and 5f superconductors, introducing the possibility of similarities with the “stripe phases” found in high T_c cuprates. Both R. Caciuffo and K. McEwen discussed higher-order multipole effects, and the important role that these can play in f–electron physics. This is demonstrated by the dynamical properties of UO₂, which are now finally understood, some 45 years after they were first measured.

Finally, Z. Fisk (U. California Irvine) summarized the challenges ahead and there was a spirited discussion of future collaborative projects, not forgetting the crucial importance of samples, often in the form of single crystals, that are needed to disentangle the complicated physics.

(10) *New in-sights combining in-situ AC susceptibility measurements with neutron spectroscopy.*

Similar to CeCoIn₅ we also investigated UBe₁₃ using inelastic neutron scattering. We established unusual longitudinally polarized spin dynamics builds up on cooling for temperatures below $T \sim 50$ K at a unique Q_0 position as a result of the competition among moment localization, exchange interactions, and magneto-crystalline anisotropy. The normal state spin dynamics reflects the energy scales observed in heat capacity measurements and determines the superconducting energy scales, i.e., T_c . On entering the superconducting state no sharp 'spin resonance' appears. Some hints for subtle changes in the spin dynamics of UBe₁₃ at Q_0 are observed comparing spectra taking above and

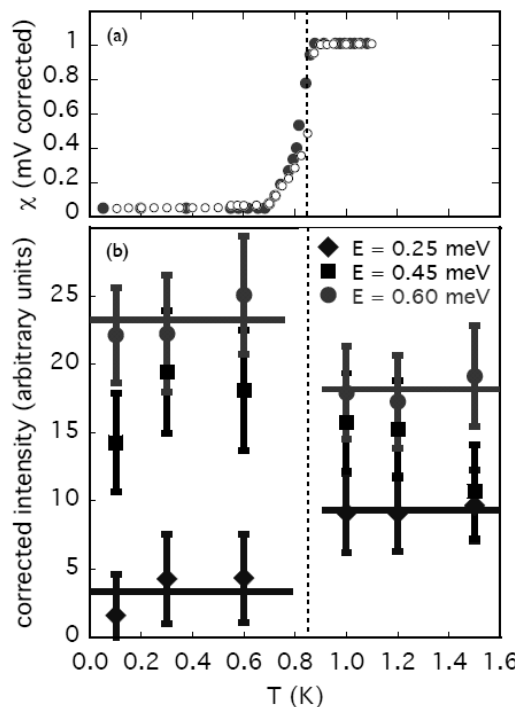


Fig. 3 Temperature dependence of (a) AC susceptibility and (b) spin dynamics measured on the same UBe₁₃ single crystal.

below the superconducting transition (Fig. 3). The unambiguous proof that the spin dynamics changes is obtained when confronting the neutron measurements with AC susceptibility measurements on the same sample and cryostat. Clearly the changes in the neutron data coincide with the transition evidenced by the AC susceptibility measurement. Those AC susceptibility measurements were performed at ILL using equipment kindly let from MPI Dresden. Thanks to the allocated budget within the REIMEI program we now acquired equipment dedicated for such measurements.

4. Conclusion

The present REIMEI program has made a good start with a consolidation in the second year of operation (2011-2012). The objective is to increase our understanding of the unusual properties of the 5f electron systems by establishing collaborations on an international scale, and performing difficult experiments at large central facilities. These have the capability of answering questions about the microscopic origins of the unusual physics of the 5f electron states.

Some examples of the work planned for the near future are given below:

- (1) Further work at JAEA on NpPd_5Al_2 to make larger crystals for neutron scattering at JRR3 with ILL collaborators. This will allow a determination of the wave-vector dependence of the spin susceptibility.
- (2) NMR will now move into the 115 materials, now that the details of the resonance are known.
- (3) NMR at ITU to explore multipolar order in mixed $\text{UO}_2 - \text{NpO}_2$ system. This will complement neutron and x-ray work already done on these systems, and establish microscopically whether the intermediate phases have a frustrated quadrupolar ordering.
- (4) It appears that the AF ordering observed in PuCoIn_5 is from an impurity phase (possibly PuIn_3 ?). However, there are still interesting experiments to be done to measure the electrical resistance as a function of pressure in PuCoIn_5 and compare with such measurements already published for PuCoGa_5 .
- (5) Growth of USn_3 crystals will be attempted at JAEA and CEA, Grenoble. In principle, the use of the inelastic scattering spectrometer at J-PARC should give important information on the momentum dependence of the magnetic fluctuations, which have already been measured by NMR at JAEA. However, at the moment J-PARC does not allow the use of uranium samples, so this administrative problem needs to be solved. Further experiments on USn_3 single crystals would be ARPES at SPring-8 – allowing a comparison of band structure calculations
- (6) Researchers from JAEA, CEA, and ILL collaborate on inelastic neutron scattering investigations. The project started with studies on cerium 115 superconductors such as CeCoIn_5 . Those compounds are precursor for future investigations planned on the newly discovered isostructural plutonium based superconductors PuCoGa_5 and PuCoIn_5 . Experimental beam time has already been granted to an ILL-JAEA-ITU group to study UPd_2Al_3 .
- (7) A further follow-up workshop is planned in 2013.

5. References

*Current address: European Spallation Source AB, Lund, Sweden.

- [1] H. Yasuoka, G. Goutroulakis, H. Chudo, S. Richmond, D. K. Veirs, A. I. Smith, E. D. Bauer, J. D. Thompson, G. D. Jarvine, and D. L. Clark, *Science* **336** 901 (2012).
- [2] E. D. Bauer, M. M. Altarawneh, P. H. Tobash, K. Gofryk, O. E. Ayala-Valenzuela, J. N. Mitchell, R. D. McDonald, C. H. Mielke, F. Ronning, J-C. Griveau, E. Colineau, R. Eloirdi, R. Caciuffo, B. L. Scott, O. Janka, S. M. Kauzlarich, and J. D. Thompson, *J. Phys. Cond. Matt.* **24** 052206 (2012).
- [3] S. Raymond, K. Kaneko, A. Hiess, P. Steffens, and G. Lapertot, submitted for publication.
- [4] H. Sakai, S. E. Brown, S-H. Baek, F. Ronning, E. D. Bauer, and J. D. Thompson, *Phys. Rev. Lett.* **107**, 137001 (2011).
- [5] H. Sakai, Y. Tokunaga, S. Kambe, H-O. Lee, V. A. Sidorov, P. H. Tobash, F. Ronning, E. D. Bauer, and J. D. Thompson, *Phys. Rev. B* **83**, 140408(R) (2011).
- [6] R. Caciuffo, P. Santini, S. Carretta, G. Amoretti, A. Hiess, N. Magnani, L.-P. Regnault, and G. H. Lander, *Phys. Rev. B* **84**, 104409 (2011).
- [7] J. P. Sanchez, D. Aoki, R. Eloirdi, P. Gaczynski, J. C. Griveau, E. Colineau, and R. Caciuffo, *J. Phys. Cond. Matt.* **23**, 295601 (2011).
- [8] S. Raymond, J. Bouchet, G. H. Lander, M. L. Tacon, G. Garbarino, M. Hoesch, J-P. Rueff, M. Krisch, J. C. Lashley, R. K. Schulze, and R. C. Albers, *Phys. Rev. Lett.* **107**, 136401 (2011).

2. New fission mechanism peculiar to proton-rich nuclei

Andrei Andreyev¹, Katsuhisa Nishio², Xavier Derkx¹, Joseph Lane¹, Valentina Liberati¹, Kalvinder Sandhu¹, Satoshi Chiba², Shin-ichi Mitsuoka², Ichiro Nishinaka², Hiroyuki Makii², Yasuo Wakabayashi², Yoshihiro Aritomo², Shuya Ota², Tatsuro Nagayama², Lars Ghys³, Tsutomu Ohtsuki⁴, IS466 and ISOLDE Collaboration (CERN, Geneva, Switzerland)

¹ School of Engineering, University of the West of Scotland, UK

² Advanced Science Research Center, Japan Atomic Energy Agency, Japan

³ IKS, KU Leuven, Belgium

⁴ Tohoku University, Japan

Abstract

In a series of complementary experiments at the tandem of JAEA and at the mass-separator ISOLDE (CERN), new fission phenomena in the very proton-rich nuclei in the lead region were investigated. At ISOLDE, the low-energy fission of ^{178}Hg and of ^{202}Rn was studied via the process of beta-delayed fission of the parent ^{178}Tl and ^{202}Fr nuclei, respectively. At JAEA the higher-energy fission studies of excited compound nuclei $^{180,184,190,194}\text{Hg}^*$ were performed in fusion-fission reactions.

1. Research Objectives

It is well known that low-energy fission data are notoriously difficult to obtain except for well-studied cases of spontaneous fission and particle-induced fission in the vicinity of beta-stability in the actinide region, see nuclei shown by open circles in Fig. 1. However, in the last decade, through technological, experimental and theoretical advances, the situation in experimental low-energy fission studies has changed dramatically. Nowadays, with the use of modern production and detection techniques we can obtain fission data for new regions of nuclei, which is characterized by the different isospin of a nucleus or neutron-to-proton ratio (N/Z). The preferential asymmetric fission fragment mass split of actinide nuclei with $N/Z \sim 1.5\text{--}1.6$ (e.g. ^{227}Ra , ^{236}U , ^{256}Fm in Fig. 1) is well understood due to the strong shell effects of the fission fragments in the vicinity of the doubly-magic ^{132}Sn ($Z = 50$, $N = 82$). In contrast to this, a transition to a predominantly symmetrical mass split was observed in the pre-actinide and light At-Ra nuclei with $N/Z \sim 1.38\text{--}1.40$ (e.g. ^{209}Ra , ^{213}At in Fig. 1). The studies of even more exotic proton-rich nuclei is important to establish what role the shell structure plays in the fission process in the region of nuclei with $N/Z \sim 1.2\text{--}1.3$ in Fig. 1.

Our collaborative program started with the observation of the β^+/EC delayed fission in several proton-rich Bi and At nuclei at GSI, Darmstadt. For example, during the irradiation with ^{56}Fe projectiles on the ^{141}Pr target, large pulse signals were recorded at the focal plane silicon

detectors of the velocity filter SHIP, which we assigned to the β^+ /EC delayed fission of ^{194}At (fission of ^{194}Po). As shown in Fig. 2, beta-delayed fission (βDF) is a two step process in which a parent nucleus undergoes β^+ /EC decay to populate excited states in the daughter isotope and then the daughter nucleus fissions. The fission probability is determined by the balance between the decay Q_{EC} -value of the parent isotope and the fission barrier B_f of the daughter nucleus. Since the excitation energy of the daughter nucleus is limited by the available Q_{EC} -value, which is typically less than 12 MeV in this region of nuclei, shells effects are preserved in the fission of proton-rich nuclei.

Motivated by this finding, we initiated a dedicated program at the ISOLDE mass separator at CERN (Geneva) to measure the fission properties of the most proton-rich nuclei in the lead region in more detail. The first case to study was the β^+ /EC-delayed fission of ^{180}Tl (fission of ^{180}Hg), as ISOLDE is capable of production of very clean and sufficiently intense sources of lightest Tl isotopes, not available anywhere else. Based on the traditional understanding of fission derived from the typical fission of the actinide nuclei with $N/Z \sim 1.5-1.6$, ^{180}Hg was expected to split into two equal fragments $^{90}\text{Zr} + ^{90}\text{Zr}$, since semi-magic zirconium-90 has the closed neutron shell $N = 50$. The result was, however, unexpected. Mercury-180 splits dominantly into fission fragments around ^{80}Kr and ^{100}Ru and shows asymmetric mass distribution as schematically indicated in Fig. 1 [1]. The results imply the new region of asymmetric fission, which occurs in proton-rich nuclei.

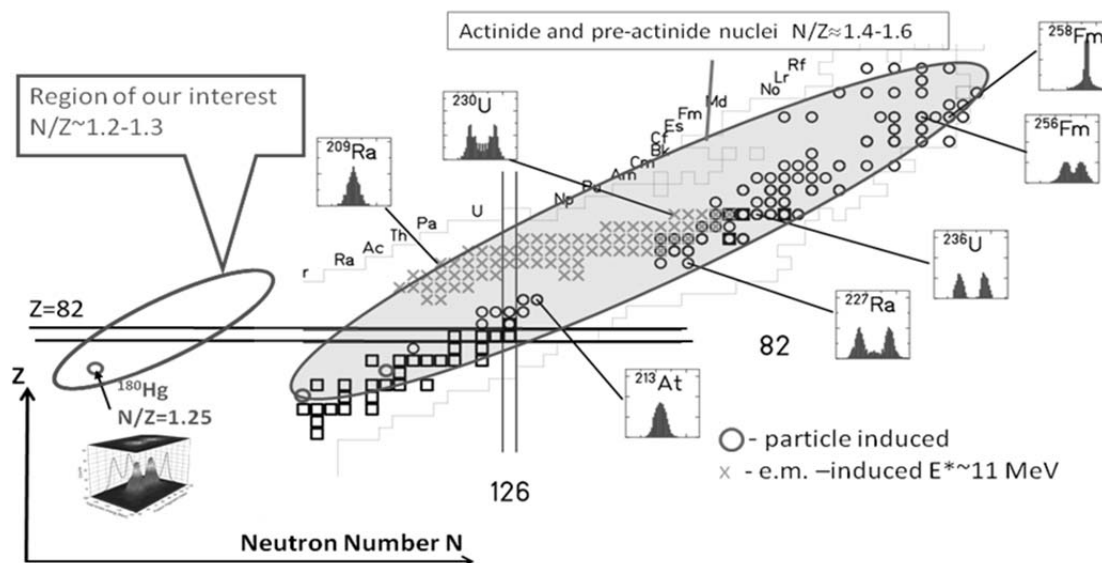


Fig. 1. The map of nuclei in the Ir-Rf ($Z = 77-104$) region with measured mass/charge distributions at low excitation energies. Most of the data on the map have been collected for the “easier-accessible” pre-actinide and actinide nuclei, located within the larger oval shape on the right and having a typical neutron-to-proton ratio of $N/Z \sim 1.4-1.6$. The particle-induced data are shown by open circles, the fission data from electromagnetically (e.m.) induced fission experiments at GSI are shown by crosses. The region of our interest is shown by an oval on the left, with a very proton rich (neutron deficient) nucleus with $N/Z \sim 1.2-1.3$. The position of ^{180}Hg ($N/Z = 1.25$), for which a surprising asymmetric mass split was found in our study at ISOLDE [1] is also shown.

By studying fission in this region, we aim to see the appearance and evolution of shell structure to regulate fission of exotic proton-rich nuclei. Since the number of nuclei available for studies by β^+ /EC delayed fission is limited, we also use heavy-ion induced fusion to populate higher-excited proton-rich nuclei. By doing this, we can cover wider region on the chart of nuclei.

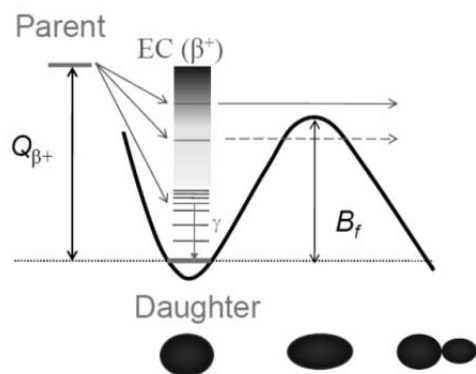


Fig. 2 Schematic presentation of the process of β^+ /EC delayed fission.

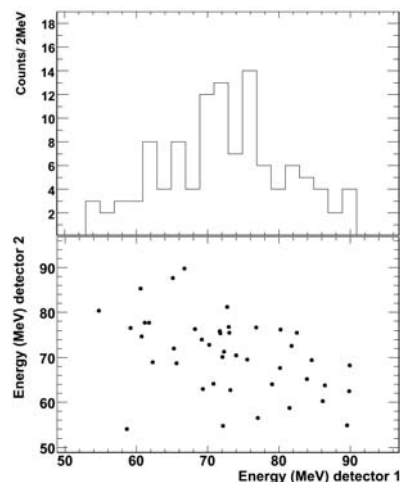


Fig. 3 The β^+ /EC delayed fission events for ^{202}Fr (fission of ^{202}Rn) [2]. Top panel – energy distribution of 112 singles fission events in Si detectors. Bottom panel – the 2D energy distribution of 43 coincident fission fragments in Si detectors.

2. Research Contents and Results

2.1 β^+ /EC delayed fission study at ISOLDE (CERN)

The β^+ /EC delayed fission was studied at ISOLDE (CERN). In our experimental campaign in 2011, we performed the beta-delayed fission studies of ^{202}Fr [2] and of ^{178}Tl [3]. A 1.4 GeV proton beam with an average intensity of 1.4 μA impinged on a 50 g/cm^2 UCx target producing a nucleus of interest. ^{202}Fr atoms were surface-ionized in the ion source, extracted and post-accelerated up to 50 keV. Following the mass separation with the High-Resolution Separator (HRS) of ISOLDE, a pure ^{202}Fr beam of ~ 90 atoms/s passed through the hole in an annular silicon detector and was implanted into a carbon foil of 20 $\mu\text{g}/\text{cm}^2$ thickness. A second Si detector was placed 3 mm behind the carbon foil. By using the two silicon detectors (both with a thickness of 300 μm), fission fragments of ^{202}Rn (being the daughter of ^{202}Fr after beta decay) were detected in singles and coincidence mode. In total, 112 singles and 43 coincident fission events were detected. The respective energy spectra are shown in Fig. 3.

In spite of the relatively low statistics, it is found that the low-energy fission of ^{202}Rn ($Z = 86$, $N = 116$, $N/Z \sim 1.35$) has a single-humped energy spectrum, which means that it has a symmetric fragment mass distribution centered around ^{100}Mo ($Z = 42$, $N = 58$, $N/Z = 1.38$) and ^{102}Ru ($Z = 44$, $N = 58$, $N/Z \sim 1.32$). On the one hand, this finding is in a clear contrast to the asymmetric mass split of ^{180}Hg , measured via beta-delayed fission of ^{180}Tl [1]. On the other hand, however, it is

important to remind that the heavier group of the fission fragments from ^{180}Hg was centered around ^{100}Ru . Therefore, it seems that the fission fragments around $^{100,102}\text{Ru}$ could play a special role in the fission of proton rich nuclei in this region.

Another important observation from the fission of ^{202}Rn is the relative broadness of energy distribution of the fission fragments and of the Total Kinetic Energy (TKE) distribution (not shown in this contribution). This hints to the fact that possibly two different fission modes contribute to the observed spectra for ^{202}Rn [2].

In a similar way, the beta-delayed fission of ^{178}Tl (fission of ^{178}Hg) was studied at ISOLDE [3]. Due to much lower production rate (~ 1 atoms/s) only 8 fission fragments were observed. Despite low statistics, the measured energy (thus mass) distribution of fission fragments of ^{178}Hg is asymmetric, similar to the case of ^{180}Hg .

2.2 Fusion-fission study at JAEA tandem facility.

We also performed fission studies at relatively higher excitation energies populated by heavy-ion induced fusion reactions. An advantage of this approach is that by choosing different combinations of projectile and target nucleus, wider variety of fissioning nuclei can be populated, allowing us to study systematic behavior of fission properties along the Chart of Nuclei. Moreover, by changing the beam energy, we can study the excitation energy dependence of the fission fragment mass distribution, and thus the transition from the low-energy fission influenced by the shell effects to the higher-energy fission where the symmetric liquid-drop behavior would be expected. For this study, we used the JAEA tandem facility at Tokai. The studies at JAEA are unique and very important for this program, as we have access to a tandem accelerator (to reach the necessary beam energy precision when moving to deep sub-barrier energies) and also the JAEA fission group possesses a two-arm fission spectrometer used for many fission studies [4]. So far, we have carried out the fission studies in the reactions $^{36,40}\text{Ar} + ^{144,154}\text{Sm} \rightarrow ^{180,184,190,194}\text{Hg}^*$ in the bombarding energies corresponding to the excitation energies of $E^* = 35 - 66$ MeV.

Figure 4 shows example of the measured fission fragment mass distributions (top) and total kinetic energy distributions (bottom) for $^{36}\text{Ar} + ^{144}\text{Sm} \rightarrow ^{180}\text{Hg}^*$ and $^{36}\text{Ar} + ^{154}\text{Sm} \rightarrow ^{190}\text{Hg}^*$. The mass distributions are well reproduced by asymmetric fission split with masses centered at $A_L/A_H = 79/101$ and $82/108$ for $^{180}\text{Hg}^*$ and $^{190}\text{Hg}^*$, respectively. As the bombarding energies for the two reactions are nearly the same, the angular momentum brought to the system (in other words - the rotational energy of the fissioning systems) is nearly the same. The fission of $^{180}\text{Hg}^*$ gives almost the same mass asymmetry as observed in the β^+/EC -delayed fission of ^{180}Tl ($A_L/A_H = 80/100$). It means that the mass asymmetry does not change much with increasing the excitation energy, and the data obtained in the fusion-fission data can be used to study the island (or peninsula) for the asymmetric fission in the proton rich nuclei. Another interesting finding in the mass distribution is that even at the excitation energy of 57 MeV in $^{190}\text{Hg}^*$ the shells are not washed out and to regulate the mass asymmetry in fission. These findings are in clear contrast to the fission of typical actinide fissions of around $N/Z = 1.5 - 1.6$.

Total kinetic energy obtained in the higher-energy fission of $^{180}\text{Hg}^*$ is 131.7 MeV, which is very close to the value obtained in the β^+/EC -delayed fission of ^{180}Tl (134 MeV) [1]. The standard

deviation of 11.7 MeV for the TKE distribution is larger than that for the β^+ /EC-delayed fission of ^{180}Tl (5.6 MeV) [1], which means that the higher temperature of the fission system does not change the average distance between the charge centers at the instant of nuclear rupture, whereas the temperature changes fluctuation of the distance.

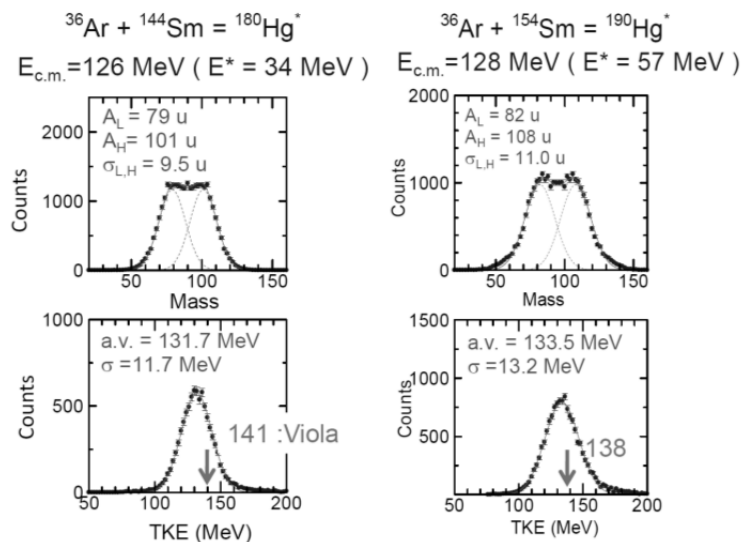


Fig. 4 Fission fragment mass and TKE distributions obtained in the reactions of $^{36}\text{Ar} + ^{144}\text{Sm} \rightarrow ^{180}\text{Hg}^*$ and $^{36}\text{Ar} + ^{154}\text{Sm} \rightarrow ^{190}\text{Hg}^*$.

3. Conclusion

In a series of ISOLDE experiment, β^+ /EC delayed fission of ^{202}Fr and of ^{178}Tl was studied. The measured kinetic energy spectra suggested the symmetric fission of ^{202}Rn with the fission fragments centered around ^{100}Mo - ^{102}Ru . As the next step in the program, we will continue experiments for the β^+ /EC-delayed fission of ^{200}Fr and of $^{194,196}\text{At}$ at ISOLDE.

At the JAEA tandem facility, in-beam fission studies in the reactions of $^{36,40}\text{Ar} + ^{144,154}\text{Sm} \rightarrow ^{180,184,190,194}\text{Hg}^*$ were carried out. We found that mass asymmetric fission is kept up to much high excitation energies than studied by beta-delayed fission at ISOLDE, so that the mass asymmetry can be studied in more detail also in the heavy-ion induced reactions. Detailed analysis on the excitation energy dependence is under analysis. As the next step at JAEA, the $^{90}\text{Zr} + ^{90}\text{Zr} \rightarrow ^{180}\text{Hg}^*$ and, later on, $^{100}\text{Ru} + ^{80}\text{Kr} \rightarrow ^{180}\text{Hg}^*$, reactions, leading to the same compound nucleus $^{180}\text{Hg}^*$ will be studied. The $^{90}\text{Zr} + ^{90}\text{Zr} \rightarrow ^{180}\text{Hg}^*$ reaction leads to a low excitation energy of $E^*(^{180}\text{Hg}) \sim 15$ MeV, which approaches the maximum excitation energy of 10.4 MeV achieved in our beta-delayed study of ^{180}Hg .

4. References

- [1] A. Andreyev *et al.*, "New type of asymmetric fission in proton-rich nuclei", *Phys. Rev. Lett.*, **105**, 252102 (2010).
- [2] L. Ghys, A. Andreyev, K. Nishio *et al.*, Private communication.
- [3] V. Liberati, A. Andreyev, K. Nishio *et al.*, Private communication.
- [4] K. Nishio *et al.*, *Phys. Rev. C*, **77**, 064607 (2008).

3. Exploration of New Biological Specific Function by Heavy Elements Stimulus

Lynne Macaskie¹, Joanna Renshaw², Toshihiko Ohnuki³, Norihiko Nishiguchi⁴, Satoshi Utsunomiya⁵, Yoshinori Suzuki⁶, and Osamu Shirai⁷

¹School of Biosciences, and ²School of Geography, University of Birmingham, UK

³Advanced Science Research Center, Japan Atomic Energy Agency, Japan

⁴Faculty of Engineering, Hokkaido University, Japan

⁵Department of Chemistry, Kyushu University, Japan

⁶School of Bioscience, Tokyo University of Technology, Japan

⁷Graduate School of Agriculture, Kyoto University, Japan

Abstract

We have carried out experiments to investigate bio-mineralization of rare earth elements (REE) on the cell surface of yeast *Saccharomyces cerevisiae*, and the bacteria *Bacillus subtilis*, *Pseudomonas fluorescens* and *Serratia* sp. The continuous removal of 1 mM La (100%) Nd (100%) and Eu(>80%) was observed using a continuous flow through immobilized *Serratia* sp cell columns. Chemical and physical characterization of bio-mineralized La and Eu was done by XRD at Birmingham and showed the formation of phosphate minerals. Additional cell column work using *S. cerevisiae*, *B. subtilis*, or *P. fluorescens*, showed that these bacteria are capable of bio-mineralizing Ce(III) and Sm(III). Chemical and physical characterizations of bio-transformed Ce and Sm were analyzed by JAEA, Kyushu U., Tokyo U. Tech. and Kyoto U. using XAFS, SEM and TEM. Results showed that Ce and Sm nanoparticles were formed. The high radiostability of the metal accumulating enzyme of *Serratia* sp. (which promotes metal phosphate deposition) was shown in whole cells, whereas pure enzyme lost its activity quickly under irradiation. Additional work on radionuclide (Cm) incorporation into *Serratia* sp calcium phosphate minerals (analogue for human bones) using EXAFS and Time Resolved Laser Fluorescence Spectroscopy (in collaboration with Karlsruhe Institute of Technology) showed that this actinide binds at the grain boundaries between crystallites, which has health implications for human exposure.

1. Research Objectives

The overall objective of the research is to explore new biological specific function and to understand this function in molecular level. To achieve this the aims are to use precious

metals, actinides (An) and rare earth elements (REE) as stimuli, focusing particularly on cerium since Ce(III) and Ce(IV) are a surrogate for An(III) and An(IV), and Ce is also a REE in its own right. We aim to focus on bio-mineralization, even though many processes of transformation are reported. Chemical and physical forms of the minerals formed by bio-transformations will be analyzed by JAEA, Kyushu U., Tokyo U. Tech., Kyoto U. by using XAFS, SEM, TEM, SANS, SAXS, EC, SEC-UVVis-RIM-ICPMS in order to find evidence of biological specific function for the transformation, and to elucidate the chemical processes responsible. In addition, we would like to apply the biological specific function to harness bioprocesses towards specific decontamination challenges resulting from the 2011 earthquake and tsunami.

2. Research Content

We used representative microorganism: yeast (*Saccharomyces cerevisiae*) and Gram positive (*Bacillus subtilis*) and Gram negative (*Pseudomonas fluorescens*, *Serratia* sp.) bacteria, 'simple' rare earth elements (Eu(III), Nd(III), Sm(III)) and multivalent ones (Ce(III)/IV) as

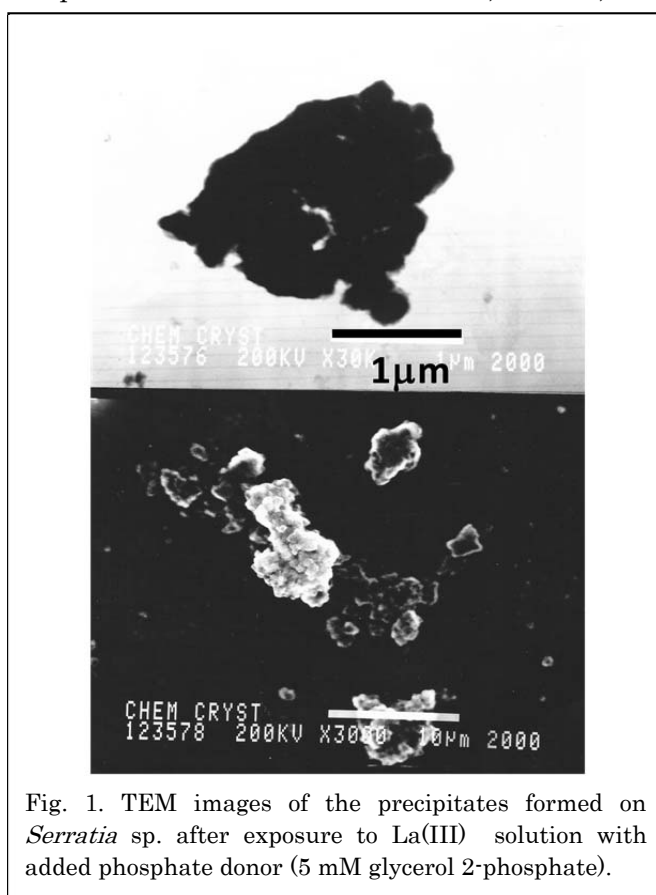


Fig. 1. TEM images of the precipitates formed on *Serratia* sp. after exposure to La(III) solution with added phosphate donor (5 mM glycerol 2-phosphate).

well as the radiotoxic actinide curium which exists predominantly as Cm(III). The microbiological systems were representative examples while the chemical systems comprised 'cold' REE surrogates for An(III)/IV) as well as a real actinide Cm(III) for cross-validation. As well as examination of the underlying molecular mechanisms of metal removal into deposited biominerals and the physical and chemical nature of the metallic deposits, the work predicted continuous stability of the system by high-dose radioactive challenge experiments and by determination of the continuous removal of the REE 'surrogates' from aqueous flows using immobilized cells in a filter arrangement.

3. Research Results

Scoping tests using *Serratia* sp. showed high radiostability of the metal-depositing phosphatase which promotes metal phosphate deposition on the cells[1]. Phosphatases are

often very robust enzymes. Exposed to a commercial ^{60}Co gamma source purified phosphatase lost activity but whole-cell enzyme radiostability was seen after more than 1000 Gy, boosting confidence towards field applications over extended periods. The same system was used to show continuous removal of 1 mM La (100%) Nd (100%) and Eu(>80%) from a continuous flow (pH 5.5) using cells immobilized as biofilm on reticulated foam sponge and supplemented with glycerol 2-phosphate (phosphate donor for the enzyme; 5 mM. La(III) was eventually removed to up to 10 times of the bacterial dry weight, with individual cells buried in crystalline precipitate (Fig. 1) identified as metal phosphate (LaPO_4) by XRD.

Further studies used *S. cerevisiae*. When a 1×10^{-4} M Ce(III) solution was contacted with cells, the soluble Ce(III) concentration decreased as a function of exposure time and more rapidly at pH 5 than at pH 3 or 4. Analysis of the cells by FESEM, TEM, and XAFS shows that needle-shaped Ce(III) phosphate nanocrystals with a monazite structure were formed on the cells by exposure to Ce(III) for 42 h (Fig. 2), even though the initial solutions did not contain any added P species. The Ce(III) phosphate nanocrystals grew from ~ 50 nm to hundreds of nm when the pH was increased from 3 to 5. A lower pH gave a higher P concentration in the solution after the yeast cells were inoculated, indicating the release of P from the cells, and indicating that sorbed Ce on the cell surfaces reacted with P released from inside the yeast cell, resulting in the formation of Ce(III) phosphate nanocrystallites.

When a 1×10^{-4} M Sm(III) solution was contacted with *S. cerevisiae*, *B. subtilis*, or *P. fluorescens*,

the concentration of Sm decreased with increased exposure time at pH 3, 4, and 5, respectively. After the first 2 h, the Sm concentration decreased quickly in all systems, and then gradually decreased to the detection limit up to 120 h at pH 4 and 5 conditions. SEM photographs and an EDS spectrum of yeast cells after exposure in Sm(III) solution for 2 h, showed that the yeast cell surface was clean without precipitate formation at

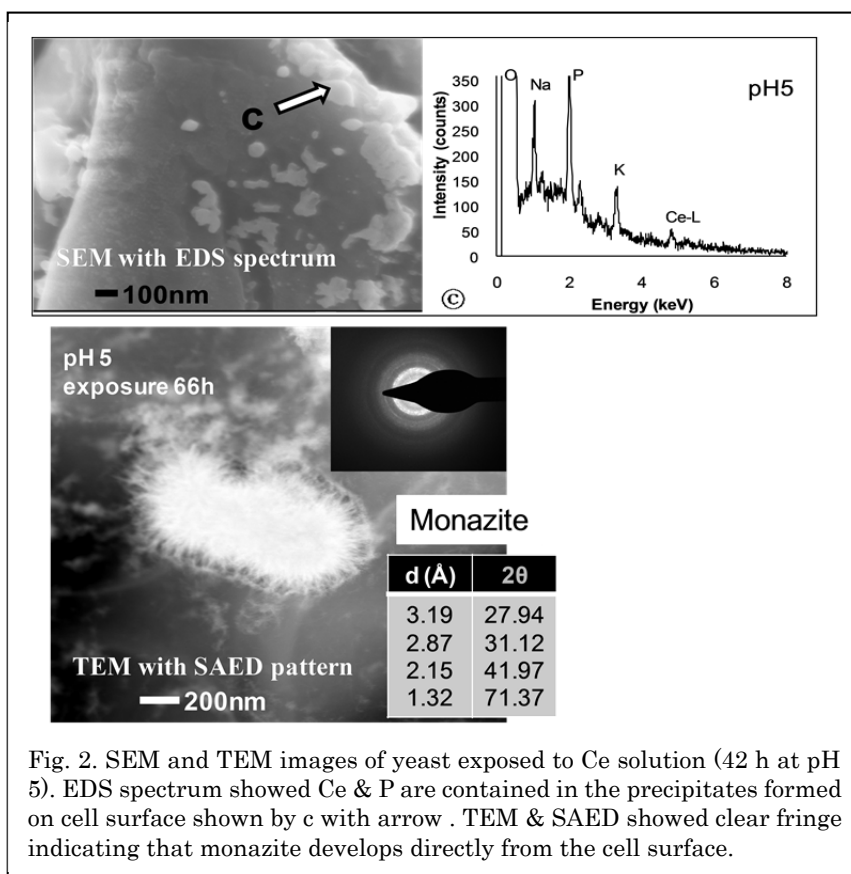


Fig. 2. SEM and TEM images of yeast exposed to Ce solution (42 h at pH 5). EDS spectrum showed Ce & P are contained in the precipitates formed on cell surface shown by c with arrow . TEM & SAED showed clear fringe indicating that monazite develops directly from the cell surface.

pH 3, 4, and 5. The decrease in the Sm concentration over 2 h indicates short-term adsorption onto yeast cell surface. Up to 24 h and 120 h, small sized precipitates were detected on the cell surface at pH 4 and pH 5. At pH 3, no precipitates formed at 24 h, but were detected after 120 h. The Sm concentration kept almost constant up to 48 h, decreasing at 96 h from the precipitation. The composition of the precipitates analyzed by EDS showed obvious Sm and P. It suggested that Sm-bearing phosphate precipitates formed on yeast cells surface, which resulted in more amount of Sm sequestering from solution in a long-term sorption process.

SEM photographs of cells of *P. fluorescens* and *B. subtilis* showed small (~100 nm) Sm-phosphate precipitates on the bacterial cell surfaces at pH 4 and 5 with the amount of precipitates increasing with exposure time to 120 h. Both in Sm/yeast and Sm/bacteria, adsorbed Sm formed Sm phosphate phase precipitates on the cell surface after short-term adsorption, similar to the Ce (light REE) precipitation process in yeast exposure system[2].

Adsorbed Sm on the cells reacted with the P released from inside cells to form the Sm-precipitates under supersaturated condition. Compared with Sm precipitation at 24 h on yeast, the formation of Sm-precipitates on bacteria was more rapid (2 h exposure at pH 4 and 5), possibly promoted by the different structure of the yeast and bacterial cell walls; yeast has a thicker cell wall, which may make it better to release P more slowly than the bacterial cells.

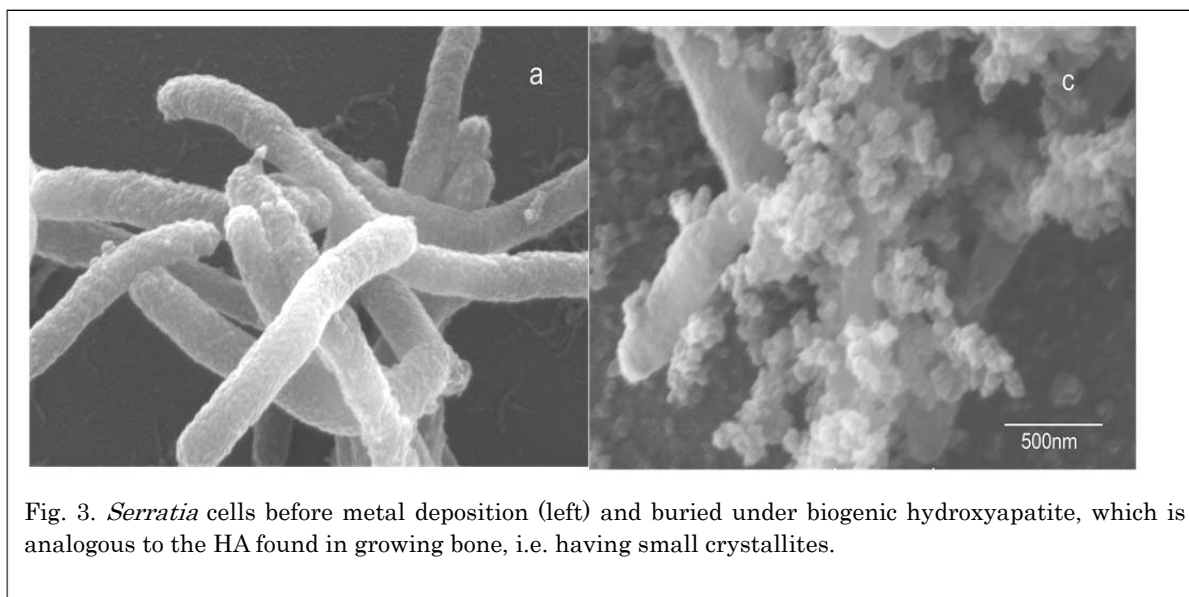


Fig. 3. *Serratia* cells before metal deposition (left) and buried under biogenic hydroxyapatite, which is analogous to the HA found in growing bone, i.e. having small crystallites.

The 'real world' will contain an excess of Ca^{2+} ions which will compete for available phosphates to make Ca-phosphates like hydroxyapatite (HA), as hybrid co-crystals with the 'target' radionuclide phosphates. Such co-crystallization helps promote removal of trace radionuclides by forming crystallization foci and making a 'host crystal' for efficient radionuclide entrapment and capture. *Serratia* cells deposited calcium phosphate identified as HA by XRD (Fig. 3). Cells were prepared with different HA crystallite sizes, down to 20 nm (approx. 6-fold smaller than commercial HA). Target metal uptake (in this case Sr^{2+} and Co^{2+})

was inversely correlated (correlation 0.9) with HA crystallite size; metals were removed from real groundwater, with stability of the biomineral against dissolution as compared to 'commercial' HA. Using Eu(III)/Cm(III) (for comparison in the REE/actinides system) and a combination of XAFS and TRLF spectroscopy, direct incorporation into the biological matrix was excluded and the incoming metal was concluded

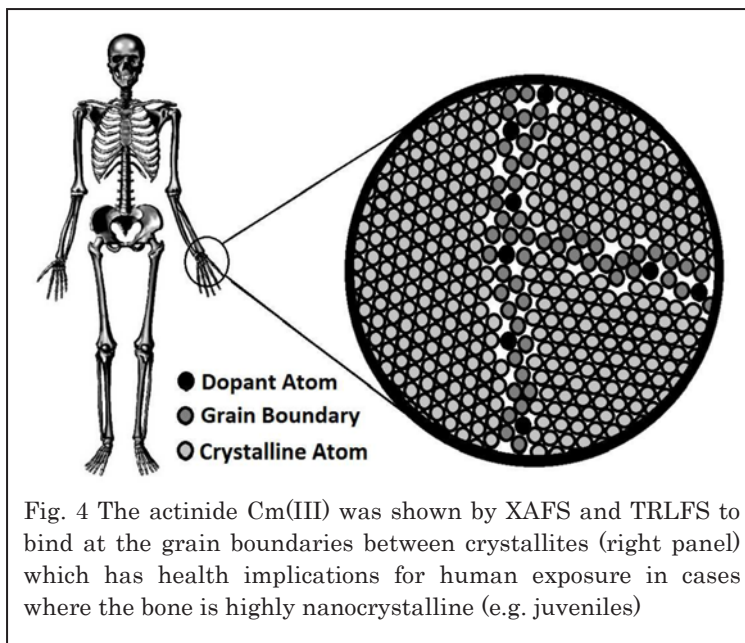


Fig. 4 The actinide Cm(III) was shown by XAFS and TRLFs to bind at the grain boundaries between crystallites (right panel) which has health implications for human exposure in cases where the bone is highly nanocrystalline (e.g. juveniles)

to bind at the grain boundaries of the host HA crystal (Fig. 4).

4. Conclusions

This study identifies the importance of biogenic metal phosphate deposition as an important, robust and durable method for removing radionuclides from solution using microbial 'filters' of several types. For high metal loads extra phosphate is supplied to the cells, but in other cases the cells require no extra feed and can generate biomineral precipitate from their own accumulated phosphate reserves. The importance of biogenic calcium phosphate (hydroxyapatite) is shown in the promotion of Cm removal and implications for human health have been revealed using the microbial model systems.

5. Acknowledgements

We acknowledge with thanks the collaboration and input of Dr K. Holliday of Karlsruhe Institute of Technology, Germany, the UK 'FENAC' facility for solid state analysis.

6. References

- [1] Paterson-Beedle M et al. *Biotech Bioeng*, **109**, 1937 (2012).
- [2] Jiang M et al. *Chem Geol*, **277**, 61(2010).

4. Synthesis, Magnetic and Transport Studies of Li(Zn,Mn)As and Other Doped I-II-V Magnets

Z. Deng¹, C. Q. Jin¹, Q. Q. Liu¹, X. C. Wang¹, J. L. Zhu¹, S. M. Feng¹, L. C. Chen¹, R. C. Yu¹,
C. Arguello², T. Goko², Fanlong Ning^{2, 3}, Jinsong Zhang⁴, Yayu Wang⁴, A. A. Aczel⁵, T. Munsie⁵,
T. J. Williams⁵, G. M. Luke⁵, T. Imai⁵, T. Kakeshita⁶, S. Uchida⁶, W. Higemoto⁷, T. U. Ito⁷,
Bo Gu^{7, 8}, S. Maekawa^{7, 8}, G. D. Morris⁹, W.Q. Yu¹⁰ and Y. J. Uemura²

¹ Beijing National Laboratory for Condensed Matter Physics, and Institute of Physics, Chinese Academy of Sciences, Beijing, China

² Department of Physics, Columbia University, New York, USA

³ Department of Physics, Zhejiang University, Hangzhou, China

⁴ Department of Physics, Tsinghua University, Beijing, China

⁵ Department of Physics and Astronomy, McMaster University, Ontario, Canada

⁶ Department of Physics, University of Tokyo, Tokyo, Japan

⁷ Advanced Science Research Center, Japan Atomic Energy Agency, Tokai, Japan

⁸ CREST, Japan Science and Technology Agency, Tokyo, Japan

⁹ TRIUMF, Vancouver, Canada

¹⁰ Department of Physics, Renmin University of China, Beijing, China

Abstract

In the Reimei project of FY 2010-11, we synthesized a new ferromagnetic system Li(Zn,Mn)As based on a I-II-V semiconductor LiZnAs and performed characterization by transport, magnetization and MuSR measurements. In FY 2011-12, we have published this discovery of new ferromagnet in Nature Communications. In addition, we synthesized a similar system Li(Cd,Mn)P and performed nuclear magnetic resonance measurements both in Li(Zn,Mn)As and Li(Cd,Mn)P.

1. Research Objectives: Introduction and background

Ferromagnetic systems obtained by doping transition metals into semiconductors [1], commonly called as Doped (or Diluted) Magnetic Semiconductors (DMS), have generated extensive studies since early 1990's [2] because of their potential use for spin-sensitive electronics (spintronics) devices. In prototypical systems based on III-V semiconductors, such as (Ga,Mn)As and (In,Mn)As, substitution of divalent Mn atoms into trivalent Ga or In sites leads to severely limited chemical solubility, resulting in chemically metastable specimens available only as epitaxial thin films [1]. Their materials quality exhibits high sensitivity on preparation methods [3], and self-doping of hole carriers via substitution prohibits electron doping. To

overcome these difficulties, Masek et al. [4] theoretically proposed systems based on a I-II-V semiconductor LiZnAs, where magnetism due to isovalent (Zn,Mn) substitution may be decoupled from carrier doping with excess/deficient Li concentrations.

Recently we succeeded in synthesizing bulk poly-crystal specimens of $\text{Li}_{1+y}(\text{Zn}_{1-x}\text{Mn}_x)\text{As}$ at the Institute of Physics (IOP) of Beijing [5]. As shown in Fig. 1, $\text{Li}(\text{Zn},\text{Mn})\text{As}$ systems exhibit ferromagnetism with T_C up to 50 K in nominally Li-excess ($y = 0.05 - 0.2$) compounds with Mn concentrations $x = 0.03-0.15$, and a very low coercive field (30-100 Oe) promising for spin manipulations. Resistivity show metallic conductivity for Li deficient and Li excess systems. The Hall resistivity exhibits anomalous Hall term due to spontaneous magnetization, and, to our surprise, p-type carriers in Li excess systems. This is likely due to excess Li substituting the Zn site and forming an acceptor.

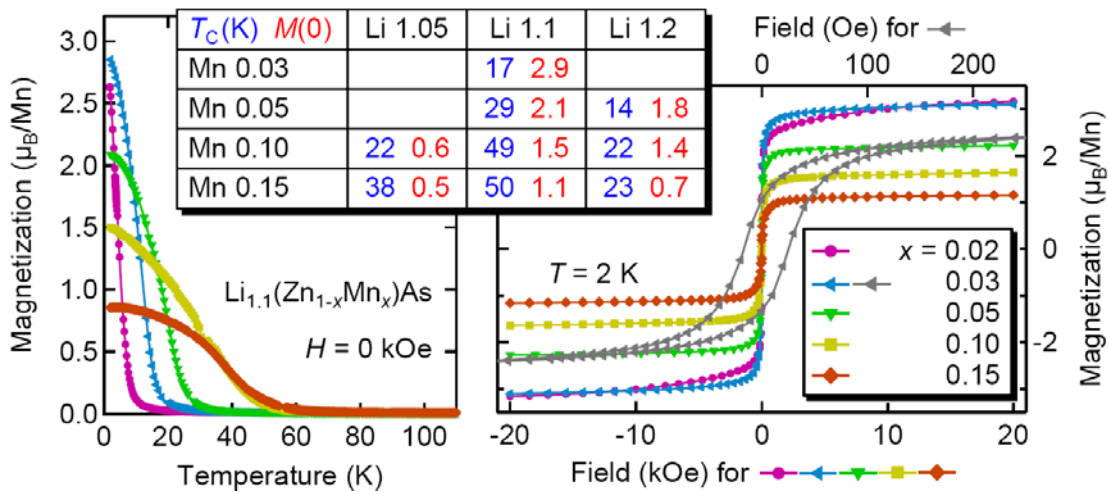


Fig.1 Magnetization $M(H)$ of $\text{Li}_{1.1}(\text{Zn}_{1-x}\text{Mn}_x)\text{As}$. The triangular symbol (\blacktriangleleft) in shows a very small coercive field of 30-100 Oe. The inset table shows the values of T_C and the average ferromagnetic ordered moment size $M(T=2\text{K};H=2\text{kOe})$ per Mn derived from magnetization measurements for nominally Li excess systems. From [5].

We performed μSR measurements in $\text{Li}_{1.1}(\text{Zn}_{0.95}\text{Mn}_{0.05})\text{As}$, and confirmed static magnetic order below $T_C \sim 27$ K, with the full volume fraction at $T = 0$ [5]. In a plot of the muon spin relaxation rate (which represent the ordered moment size times concentration) and T_C , the results from $\text{Li}(\text{Zn},\text{Mn})\text{As}$ and $(\text{Ga},\text{Mn})\text{As}$ [6] exhibit a common slope, which suggests a common ferromagnetic interactions. These results are consistent with Local Density Approximation and quantum Monte-Carlo calculations by Gu and Maekawa.

As shown in Fig. 2, ferromagnetic $\text{Li}(\text{Zn},\text{Mn})\text{As}$ ($T_C \sim 50\text{K}$) and semiconducting LiZnAs have a crystal structure similar to those of antiferromagnetic LiMnAs ($T_N \sim 450$ K) and superconducting LiFeAs ($T_{sc} \sim 25$ K), having common square-lattice As layers with 10 % lattice constants matching. This feature may enable fabrication of junction devices of various combinations of these systems for spin-sensitive electronics.

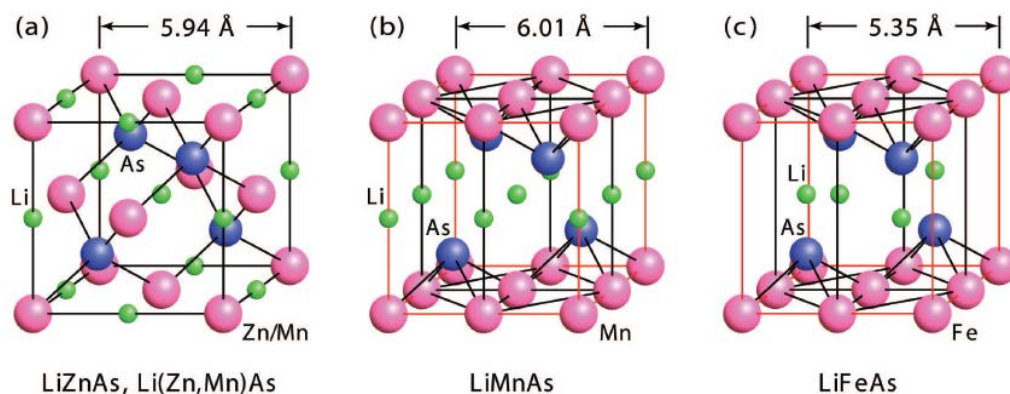


Fig. 2 Crystal structures of semiconducting LiZnAs, ferromagnetic Li(Zn,Mn)As, antiferromagnetic LiMnAs and superconducting LiFeAs.

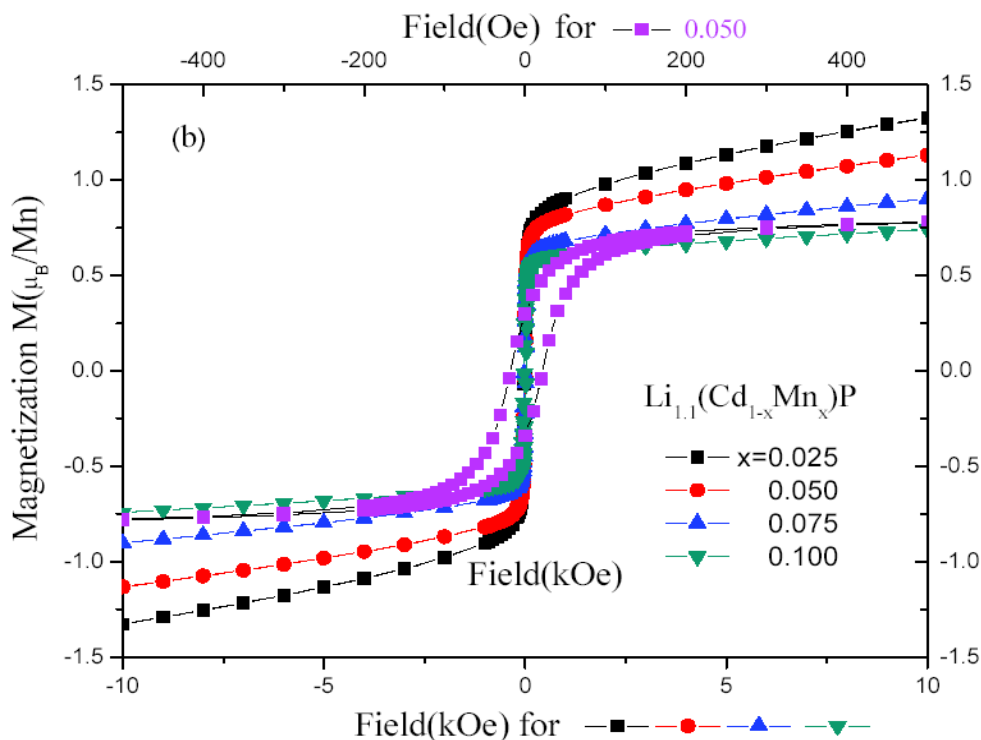


Fig. 3 Magnetization hysteresis curve $M(H)$ observed in $\text{Li}_{1.1}(\text{Cd}_{1-x}\text{Mn}_x)\text{P}$ at $T = 2\text{K}$.

2. Research Contents and Results:

I. Synthesis of a new ferromagnet system $\text{Li}(\text{Cd},\text{Mn})\text{P}$ based on a I-II-V semiconductor LiCdP

During FY 2011-12, a new system $\text{Li}(\text{Ca},\text{Mn})\text{P}$ was synthesized and characterized at IOP in Beijing. Most of the basic magnetic properties are similar to those in $\text{Li}(\text{Zn},\text{Mn})\text{As}$, and ferromagnetism was found with the Curie temperature T_c up to $\sim 50\text{K}$ for systems with excess Li concentrations. As shown in Fig. 3, the size of saturation moment was about 1 Bohr magneton per Mn, and a very small coercive field of $\sim 50\text{G}$ was observed in the magnetization hysteresis curve $M(H)$ at $T = 2\text{K}$. The Hall effect measurements confirmed positive hole carriers,

which indicates that the carriers are most-likely due to Li atoms occupying Cd sites. Although most of the magnetic and transport results are similar to those of Li(Zn,Mn)As, the new Li(Cd,Mn)P system is different from the previous Li(Zn,Mn)As in allowing to avoid usage of toxic As in the material.

II. NMR measurements of Li(Zn,Mn)As and Li(Cd,Mn)P

The availability of bulk specimens allowed NMR studies in these two systems with signals from ^7Li and ^{31}P nuclei. The Li NMR in Li(Zn,Mn)As exhibits sharp peaking of the relaxation rate $1/T_1$ at the ferromagnetic transition temperature T_C as shown in Fig. 4. The observed scaling of $1/T_1T$ with $1/(T+T_w)$, appearing with a positive T_w in a wide temperature region above T_C , suggests an influence of antiferromagnetic coupling between Mn moments located in the nearest-neighbor geometry.

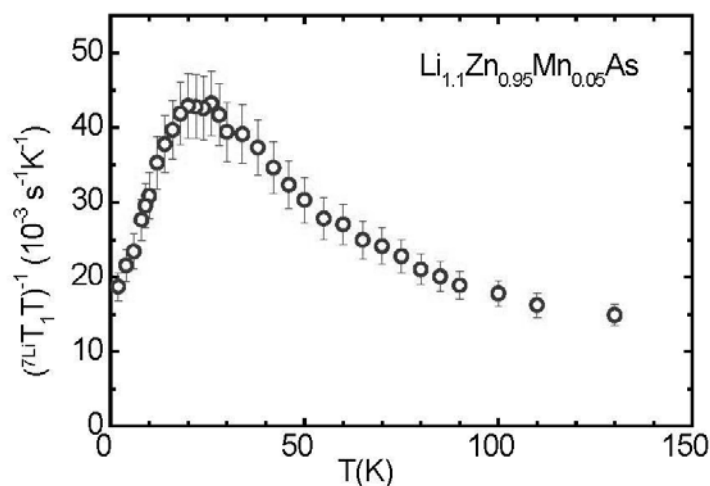


Fig. 4 The ^7Li nuclear spin relaxation rate $1/T_1$ in $\text{Li}_{1.1}\text{Zn}_{0.95}\text{Mn}_{0.05}\text{As}$ shown in a plot of $1/T_1T$ versus temperature T .

3. Conclusions and Outlooks

The results in Li(Zn,Mn)As and Li(Cd,Mn)P indicate that a wide range of ferromagnetic systems can be generated doping transition metal atoms in I-II-V semiconductors. The availability of bulk specimens is a distinct advantage over counterpart DMS systems based on III-V semiconductors. Successful measurements of NMR in Li(Zn,Mn)As and Li(Cd,Mn)P clearly demonstrate this advantage. NMR of P probes systems at different crystallographic sites from that of Li. Hence P NMR studies in Li(Cd,Mn)P may reveal new features additional to the results of Li NMR. Currently an effort is underway to generate single crystal specimens. Once crystals with sufficient size become available, neutron scattering studies can also be performed. NMR, MuSR and neutron studies using bulk specimens would certainly enrich magnetic characterizations of ferromagnetic DMS systems.

Acknowledgement:

This work has been financially supported by the REIMEI grant from JAEA of Japan,

Materials World Network and Partnership for International Research and Education projects of US-National Science Foundation, NSERC of Canada, and Chinese NSF and Ministry of Science and Technology (MOST).

4. References

- [1] H. Ohno, *Science* **281**, 951 (1998).
- [2] T. Dietl, *Nature Materials* **9**, 965 (2010).
- [3] S.J. Potashnik *et al.*, *Appl. Phys. Lett.* **79**, 1495 (2001).
- [4] J. Masek *et al.*, *Phys. Rev. Lett.* **98**, 067202 (2007).
- [5] Z. Deng *et al.*, *Nature Communications*, **2**, 422 (2011). DOI: 10.1038/ncomms1425.
- [6] S.R. Dunsiger *et al.*, *Nature Materials* **9**, 299 (2010).

5. Theory of Spintronics and materials: mechanisms and applications of the spin Hall effect, Multiferroics and Muon Spintronics

Timothy Ziman¹ and Michiyasu Mori²

¹Institut Laue Langevin and CNRS, Grenoble, France

²Advanced Science Research Center, Japan Atomic Energy Agency, Japan

Abstract

The purpose of the project was to understand mechanisms underlying the material design of devices useful in spintronics and other multifunctional materials. New directions include the applications of inverse spin Hall effects to probe nonlinear magnetic susceptibilities and investigating mechanisms for the use of muon precession to measure conduction electron spin polarizations in out of equilibrium semiconductors.

1. Research Objectives

The purpose was to reinforce efforts to understand mechanisms underlying the material design of devices useful in spintronics and other multifunctional materials. Of particular interest was the understanding of new mechanisms for enhanced spin-dependent skew scattering essential to the design of applicable inverse spin Hall effects devices. A new direction was to seek a theoretical underpinning for novel applications of muon precession to probe conduction electron spin polarizations in out of equilibrium semiconductors. This program was undertaken in close contact with relevant experimental groups with the purpose of explaining existing results and hopefully to suggest new experiments useful for either applications or better understanding of underlying mechanisms.

2. Research Contents

The specific projects in the project included the following:

(1) Enhanced skew scattering and microscopic mechanisms of the spin Hall effect.

Calculations of the spin Hall angle for conduction electrons coupled to a magnetic lattice were proposed to test the prediction that the inverse spin Hall effect can be used to probe nonlinear susceptibilities in the critical region of a ferromagnet and other magnetic materials

(2) Theory of muonium as a probe of conduction electron polarization. This work was undertaken in response to experimental results of the Nagamine / Shimomura / Torikai (KEK/JAEA/Yamanashi) muon group who made the surprising discovery that muon spin resonance can detect the spin polarization of conduction electrons in n-type doped GaAs.

Calculations were proposed to understand the fundamental mechanism that could explain this observation, interpreted by the experimentalists in that negatively charged muonium ions can detect the conduction electron spin density.

(3) The dynamics of a model multi-ferroic magnetic material $MnWO_4$ examined to better understand the role of spin-orbit interactions and the origin of the multiferroic phase. This is a project with experimentalists where inelastic neutron and X-ray data are still being obtained and the intermediary results will not be presented in the following.

3. Research results

(1) Derivation of anomalous and spin-Hall effects from microscopic spin-orbit coupling.

These effects are useful both for applications in novel spintronics devices. Spin-orbit effects, as relativistic corrections, are intrinsically weak, especially in light atoms, and it is important to find ways of enhancing their effects. In past work we have looked theoretically at the effects of quantum fluctuations of magnetic impurities to enhance spin-dependent skew scattering and this leads to a better quantitative understanding of the role of different impurities both in the bulk and, in the case of Pt impurities in gold, at the surface[2].

More recently, the group of Otani (ISSP, Kashiwa) [3] took the step of investigating the effect on the inverse spin Hall effect of *cooperative* thermal fluctuations close to the Curie temperatures in ferromagnetic nano-wires. This necessitated a theory to explain the observed anomaly. Contribution of magnetic fluctuations can become increasingly significant as we approach the Curie temperature and these can affect the skew scattering. The understanding of such effects had not advanced, and had been rather forgotten, since the classic calculations of Kondo in the early 60s [1] to estimate the fluctuation-induced contribution to the anomalous Hall coefficient.

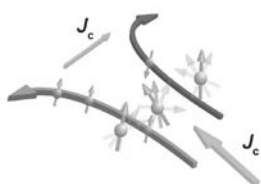


Fig. 1A The anomalous Hall effect depends on a three-spin correlation function

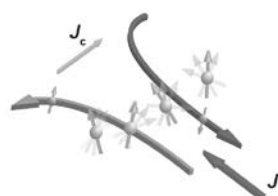


Fig. 1B The spin Hall Effect depends on a 4-spin correlation function.

We re-examined the question and showed that the calculation has to be extended to fully account for the new data, in particular of the inverse spin Hall Effect[3, 4]. Even for the anomalous Hall Effect there are extensions to the classic Kondo calculation which may be necessary to account for new and more accurate measurements, for example in Ni and Ni alloys. In the work of Kondo, the local moments fluctuate and, via the spin-orbit coupling, this leads to skew scattering. He included purely local fluctuations with the thermodynamics calculated within molecular field theory. Such excitations, classified as “extrinsic” in the sense that the transverse coefficients will have a linear dependence on the longitudinal resistance, but

“intrinsic” in the sense that these are properties of perfectly pure and crystalline materials, will be strongest in the vicinity of the Curie temperature. This is where molecular field theory is least accurate. We then extended Kondo’s theory of skew scattering coefficients to include more fully critical fluctuations and extracted the components which are independent (Fig. 1A) or dependent (Fig. 1B) on spin. Monte Carlo estimates of the higher order spin correlations for Heisenberg spins that enter the generalized expressions for the transport coefficients that we have derived are shown in Fig. 2. They show, the change of slope seen in the experimental curves of Ref 3.

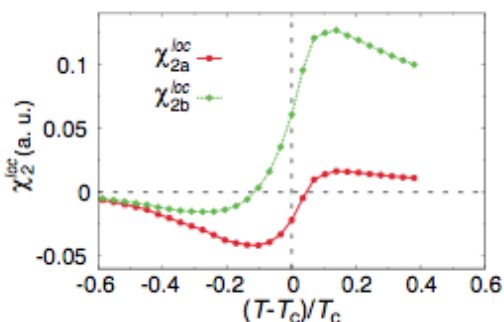


Fig. 2 The spin Hall resistivity is predicted to be a sum over 4-spin, two-site correlation functions, with different pairings on nearest neighbour sites defining χ^{loc}_{2a} and χ^{loc}_{2b} [3]. Anomalies near the Curie temperature are seen in Monte Carlo simulations.

(2) *Theory of muonium as a probe of conduction electron polarization.*

Recent experiments by the group of K. Nagamine, K. Shimomura (KEK) and E. Torikai (Yamanashi) at J-PARC have raised the issue of calculating spin dependent scattering from bound states of the Muonium⁻ ions formed in doped GaAs by the capture of a pair of conduction electrons by a positive muon. The theoretical challenge is to make quantitative estimates of both the spin-dependent scattering of conduction electrons and the scattering potential of the bound ion and the spin-flip rate of the positive muon at the centre of the Muonium “ion”, which is coupled via the hyperfine interaction to the electrons. This can be formulated in the terms of the spin-dependent phase shifts of the electron from the Muonium⁻ ion, as well as a perturbative treatment of the spin-orbit and hyperfine interactions. The theoretical challenge is to see whether resonant effects, for example, quasi-bound excited states of Muonium⁻, can produce an amplification of the effects of the hyperfine interaction. An open question is whether a treatment of the scattering in a vacuum is adequate, or whether the properties of the GaAs matrix are central. In Fig. 3. we show calculations of the local electronic structure around the muon using Gaussian bases.

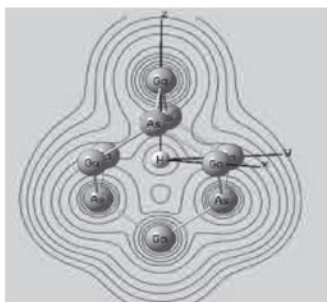


Fig. 3 Calculation of electron densities by Bo Gu for a Mu⁻ in an AsF₆ fragment of the GaAs lattice.

4. Conclusion

The Reimei project was extremely useful in seeding enduring collaborations between the different national partners and also between the theoretical members and several different experimental groups, primarily in Japan, but also, for the case of the multiferroics, in Europe. The project also was vital in the organization of the joint meeting in Tokai in January 2012 with the Reimei project directed by Prof. Uemura, postponed from March 2011.

5. References

- [1] “Anomalous Hall Effect and Magnetoresistance of Ferromagnetic Metals”, J. Kondo, Prog. Theor. Phys. **27**, 772-792 (1962).
- [2] “Surface-assisted spin Hall effect in Au films with Pt impurities”, B. Gu, I. Sugai, T. Ziman, G. Y. Guo, N. Nagaosa, T. Seki, K. Takanashi, and S. Maekawa, Phys. Rev. Lett. **105**, 216401 (2010).
- [3] “The spin Hall effect as a probe of nonlinear spin fluctuations”, D. Wei , B. Gu , T. Ziman , S. Maekawa , Y. Otani, private communication.
- [4] “Theory of the Spin Hall effect in a ferromagnetic metal near the Curie temperature”, B. Gu,T. Ziman, and S. Maekawa , private communication.

This is a blank page.

国際単位系 (SI)

表1. SI基本単位

| 基本量 | SI基本単位 | |
|-------|--------|-----|
| | 名称 | 記号 |
| 長さ | メートル | m |
| 質量 | キログラム | kg |
| 時間 | 秒 | s |
| 電流 | アンペア | A |
| 熱力学温度 | ケルビン | K |
| 物質 | モル | mol |
| 光 | カンデラ | cd |

表2. 基本単位を用いて表されるSI組立単位の例

| 組立量 | SI基本単位 | |
|-------------------------|--------------|--------------------|
| | 名称 | 記号 |
| 面積 | 平方メートル | m ² |
| 体積 | 立方メートル | m ³ |
| 速度 | メートル毎秒 | m/s |
| 加速度 | メートル毎秒毎秒 | m/s ² |
| 波数 | 数メートル | m ⁻¹ |
| 密度, 質量密度 | キログラム毎立方メートル | kg/m ³ |
| 面積密度 | キログラム毎平方メートル | kg/m ² |
| 比体積 | 立方メートル毎キログラム | m ³ /kg |
| 電流密度 | アンペア毎平方メートル | A/m ² |
| 磁界の強さ | アンペア毎メートル | A/m |
| 量濃度 ^(a) , 濃度 | モル毎立方メートル | mol/m ³ |
| 質量濃度 | キログラム毎立法メートル | kg/m ³ |
| 輝度 | カンデラ毎平方メートル | cd/m ² |
| 屈折率 ^(b) | (数字の) 1 | 1 |
| 比透磁率 ^(b) | (数字の) 1 | 1 |

(a) 量濃度 (amount concentration) は臨床化学の分野では物質濃度 (substance concentration) ともよばれる。
 (b) これらは無次元量あるいは次元1をもつ量であるが、そのことを表す単位記号である数字の1は通常は表記しない。

表3. 固有の名称と記号で表されるSI組立単位

| 組立量 | SI組立単位 | | | |
|-------------------------------|-----------------------|-------------------|-------------------|--|
| | 名称 | 記号 | 他のSI単位による表し方 | SI基本単位による表し方 |
| 平面角 | ラジアン ^(b) | rad | 1 ^(b) | m/m |
| 立体角 | ステラジアン ^(b) | sr ^(c) | 1 ^(b) | m ² /m ² |
| 周波数 | ヘルツ ^(d) | Hz | 1 | s ⁻¹ |
| 力 | ニュートン | N | | m kg s ⁻² |
| 圧力, 応力 | パスカル | Pa | N/m ² | m ⁻¹ kg s ⁻² |
| エネルギー, 仕事, 熱量 | ジュール | J | N m | m ² kg s ⁻² |
| 仕事率, 工率, 放射 | ワット | W | J/s | m ² kg s ⁻³ |
| 電荷, 電気量 | クーロン | C | | s A |
| 電位差 (電圧), 起電力 | ボルト | V | W/A | m ² kg s ⁻³ A ⁻¹ |
| 静電容量 | ファラド | F | C/V | m ⁻² kg ⁻¹ s ⁴ A ² |
| 電気抵抗 | オーム | Ω | V/A | m ² kg s ⁻³ A ⁻² |
| コンダクタンス | ジーメンズ | S | A/V | m ⁻² kg ⁻¹ s ³ A ² |
| 磁束密度 | ウェーバ | Wb | Vs | m ² kg s ⁻² A ⁻¹ |
| 磁束 | テスラ | T | Wb/m ² | kg s ⁻² A ⁻¹ |
| インダクタンス | ヘンリー | H | Wb/A | m ² kg s ⁻² A ⁻² |
| セルシウス温度 | セルシウス度 ^(e) | °C | | K |
| 光照射度 | ルーメン | lm | | cd sr ^(c) |
| 放射線核種の放射能 ^(f) | ベクレル ^(d) | Bq | | s ⁻¹ |
| 吸収線量, 比エネルギー分与, カーマ | グレイ | Gy | J/kg | m ² s ⁻² |
| 線量当量, 周辺線量当量, 方向性線量当量, 個人線量当量 | シーベルト ^(g) | Sv | J/kg | m ² s ⁻² |
| 酸素活性 | カタール | kat | | s ⁻¹ mol |

(a) SI接頭語は固有の名称と記号を持つ組立単位と組み合わせても使用できる。しかし接頭語を付した単位はもはやコヒーレントではない。
 (b) ラジアンとステラジアンは数字の1に対する単位の特別な名称で、量についての情報をつたえるために使われる。実際には、使用する時には記号rad及びsrが用いられるが、習慣として組立単位としての記号である数字の1は明示されない。
 (c) 測光学ではステラジアンという名称と記号srを単位の表し方の中に、そのまま維持している。
 (d) ヘルツは周期現象についてのみ、ベクレルは放射性核種の統計的過程についてのみに使用される。
 (e) セルシウス度はケルビンの特別な名称で、セルシウス温度を表すために使用される。セルシウス度とケルビンの単位の大きさは同一である。したがって、温度差や温度間隔を表す数値はどちらの単位で表しても同じである。
 (f) 放射性核種の放射能 (activity referred to a radionuclide) は、しばしば誤った用語で"radioactivity"と記される。
 (g) 単位シーベルト (PV,2002,70,205) についてはCIPM勧告2 (CF-2002) を参照。

表4. 単位の中に固有の名称と記号を含むSI組立単位の例

| 組立量 | SI組立単位 | | |
|-----------------|-------------------|-----------------------|--|
| | 名称 | 記号 | SI基本単位による表し方 |
| 粘り | パスカル秒 | Pa s | m ⁻¹ kg s ⁻¹ |
| 力のモーメント | ニュートンメートル | N m | m ² kg s ⁻² |
| 表面張力 | ニュートン毎メートル | N/m | kg s ⁻² |
| 角速度 | ラジアン毎秒 | rad/s | m m ⁻¹ s ⁻¹ =s ⁻¹ |
| 角加速度 | ラジアン毎秒毎秒 | rad/s ² | m m ⁻¹ s ⁻² =s ⁻² |
| 熱流密度, 放射照度 | ワット毎平方メートル | W/m ² | kg s ⁻³ |
| 熱容量, エントロピー | ジュール毎ケルビン | J/K | m ² kg s ⁻² K ⁻¹ |
| 比熱容量, 比エントロピー | ジュール毎キログラム毎ケルビン | J/(kg K) | m ² s ⁻² K ⁻¹ |
| 比エントロピー | ジュール毎キログラム | J/kg | m ² s ⁻² |
| 熱伝導率 | ワット毎メートル毎ケルビン | W/(m K) | m kg s ⁻³ K ⁻¹ |
| 体積エネルギー | ジュール毎立方メートル | J/m ³ | m ⁻¹ kg s ⁻² |
| 電界の強さ | ボルト毎メートル | V/m | m kg s ⁻³ A ⁻¹ |
| 電荷密度 | クーロン毎立方メートル | C/m ³ | m ⁻³ s A |
| 電表面積電荷 | クーロン毎平方メートル | C/m ² | m ⁻² s A |
| 電束密度, 電気変位 | クーロン毎平方メートル | C/m ² | m ⁻² s A |
| 誘電率 | ファラド毎メートル | F/m | m ⁻³ kg ⁻¹ s ⁴ A ² |
| 透磁率 | ヘンリー毎メートル | H/m | m kg s ⁻² A ⁻² |
| モルエネルギー | ジュール毎モル | J/mol | m ² kg s ⁻² mol ⁻¹ |
| モルエントロピー, モル熱容量 | ジュール毎モル毎ケルビン | J/(mol K) | m ² kg s ⁻² K ⁻¹ mol ⁻¹ |
| 照射線量 (X線及びγ線) | クーロン毎キログラム | C/kg | kg ⁻¹ s A |
| 吸収線量 | グレイ毎秒 | Gy/s | m ² s ⁻³ |
| 放射強度 | ワット毎ステラジアン | W/sr | m ³ m ⁻² kg s ⁻³ =m ² kg s ⁻³ |
| 放射輝度 | ワット毎平方メートル毎ステラジアン | W/(m ² sr) | m ² m ⁻² kg s ⁻³ =kg s ⁻³ |
| 酵素活性濃度 | カタール毎立方メートル | kat/m ³ | m ⁻³ s ⁻¹ mol |

表5. SI接頭語

| 乗数 | 接頭語 | 記号 | 乗数 | 接頭語 | 記号 |
|------------------|-----|----|------------------|------|----|
| 10 ²⁴ | ヨタ | Y | 10 ¹ | デシ | d |
| 10 ²¹ | ゼタ | Z | 10 ² | センチ | c |
| 10 ¹⁸ | エクサ | E | 10 ³ | ミリ | m |
| 10 ¹⁵ | ペタ | P | 10 ⁶ | マイクロ | μ |
| 10 ¹² | テラ | T | 10 ⁹ | ナノ | n |
| 10 ⁹ | ギガ | G | 10 ¹² | ピコ | p |
| 10 ⁶ | メガ | M | 10 ¹⁵ | フェムト | f |
| 10 ³ | キロ | k | 10 ¹⁸ | アト | a |
| 10 ² | ヘクト | h | 10 ²¹ | ゼプト | z |
| 10 ¹ | デカ | da | 10 ²⁴ | ヨクト | y |

表6. SIに属さないが、SIと併用される単位

| 名称 | 記号 | SI単位による値 |
|-------|------|--|
| 分 | min | 1 min=60s |
| 時 | h | 1 h=60 min=3600 s |
| 日 | d | 1 d=24 h=86 400 s |
| 度 | ° | 1°=(π/180) rad |
| 分 | ' | 1'=(1/60)°=(π/10800) rad |
| 秒 | " | 1"=(1/60)'=(π/648000) rad |
| ヘクタール | ha | 1ha=1hm ² =10 ⁴ m ² |
| リットル | L, l | 1L=11=1dm ³ =10 ³ cm ³ =10 ⁻³ m ³ |
| トン | t | 1t=10 ³ kg |

表7. SIに属さないが、SIと併用される単位で、SI単位で表される数値が実験的に得られるもの

| 名称 | 記号 | SI単位で表される数値 |
|----------|----|--|
| 電子ボルト | eV | 1eV=1.602 176 53(14)×10 ⁻¹⁹ J |
| ダルトン | Da | 1Da=1.660 538 86(28)×10 ⁻²⁷ kg |
| 統一原子質量単位 | u | 1u=1 Da |
| 天文単位 | ua | 1ua=1.495 978 706 91(6)×10 ¹¹ m |

表8. SIに属さないが、SIと併用されるその他の単位

| 名称 | 記号 | SI単位で表される数値 |
|-----------|------|---|
| バール | bar | 1 bar=0.1MPa=100kPa=10 ⁵ Pa |
| 水銀柱ミリメートル | mmHg | 1mmHg=133.322Pa |
| オングストローム | Å | 1 Å=0.1nm=100pm=10 ⁻¹⁰ m |
| 海里 | M | 1 M=1852m |
| バイン | b | 1 b=100fm ² =(10 ⁻¹² cm ²)=10 ⁻²⁸ m ² |
| ノット | kn | 1 kn=(1852/3600)m/s |
| ネーパ | Np | SI単位との数値的な関係は、 対数量の定義に依存。 |
| ベベル | B | |
| デジベル | dB | |

表9. 固有の名称をもつCGS組立単位

| 名称 | 記号 | SI単位で表される数値 |
|-----------------------|-----|--|
| エル | erg | 1 erg=10 ⁻⁷ J |
| ダイン | dyn | 1 dyn=10 ⁻⁵ N |
| ポアズ | P | 1 P=1 dyn s cm ⁻² =0.1Pa s |
| ストークス | St | 1 St=1cm ² s ⁻¹ =10 ⁻⁴ m ² s ⁻¹ |
| ストルブ | sb | 1 sb=1cd cm ⁻² =10 ⁻⁴ cd m ⁻² |
| フォト | ph | 1 ph=1cd sr cm ⁻² 10 ⁴ lx |
| ガリ | Gal | 1 Gal=1cm s ⁻² =10 ⁻² ms ⁻² |
| マクスウェル | Mx | 1 Mx=1G cm ² =10 ⁸ Wb |
| ガウス | G | 1 G=1Mx cm ⁻² =10 ⁻⁴ T |
| エルステッド ^(c) | Oe | 1 Oe ≡ (10 ³ /4π)A m ⁻¹ |

(c) 3元系のCGS単位系とSIでは直接比較できないため、等号「≡」は対応関係を示すものである。

表10. SIに属さないその他の単位の例

| 名称 | 記号 | SI単位で表される数値 |
|-----------|------|--|
| キュリー | Ci | 1 Ci=3.7×10 ¹⁰ Bq |
| レントゲン | R | 1 R=2.58×10 ⁻⁴ C/kg |
| ラド | rad | 1 rad=1cGy=10 ⁻² Gy |
| レム | rem | 1 rem=1cSv=10 ⁻² Sv |
| ガンマ | γ | 1 γ=1 nT=10 ⁻⁹ T |
| フェルミ | fm | 1 fm=10 ⁻¹⁵ m |
| メートル系カラット | | 1メートル系カラット=200 mg=2×10 ⁻⁴ kg |
| トル | Torr | 1 Torr=(101 325/760) Pa |
| 標準大気圧 | atm | 1 atm=101 325 Pa |
| カロリ | cal | 1cal=4.1858J (「15°C」カロリ), 4.1868J (「IT」カロリ), 4.184J (「熱化学」カロリ) |
| マイクロン | μ | 1 μ=1μm=10 ⁻⁶ m |

